Bioorg. Med. Chem. 72 (2022) 116969

Contents lists available at ScienceDirect

Bioorganic & Medicinal Chemistry

journal homepage: www.elsevier.com/locate/bmc

Design, synthesis and evaluation of ^{15}N- and ^{13}C-labeled molecular probes as hyperpolarized nitric oxide sensors

Hyejin Park [a,1], Shannon Eriksson [a,b,1], Warren S. Warren [a,c,*], Qiu Wang [a,*]

[a] Department of Chemistry, Duke University, Durham, NC 27708, USA
[b] School of Medicine, Duke University, Durham, NC 27708, USA
[c] Department of Physics, Radiology and Biomedical Engineering, Duke University, Durham, NC 27708, USA

ARTICLE INFO

Keywords:
Nitric oxide
Hyperpolarized nuclear magnetic resonance
^{15}N HP-NMR
^{13}C HP-NMR
Reaction-based imaging

ABSTRACT

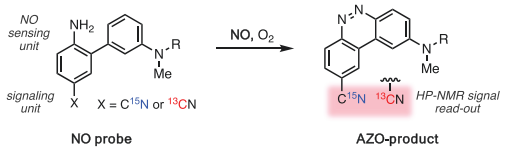

Nitric oxide (NO) is an important signaling molecule involved in a wide range of biological processes. Development of non-invasive, real-time detection of NO is greatly desired yet remains challenging. Here we report the design and development of novel ^{15}N- and ^{13}C-labeled NO-sensing probes for hyperpolarized nuclear magnetic resonance (HP-NMR) studies. These probes undergo selective and rapid reaction with NO to generate *in situ* AZO-products that can be monitored with distinguishable NMR signals as a read-out. This study also allows for a direct comparison of the ^{15}N and ^{13}C nuclei performances in hyperpolarized reaction-based probes. The simple and general SABRE-SHEATH hyperpolarization method works on the ^{15}N- and ^{13}C-NO-sensing probes. Measured long spin–lattice relaxation (T_1) values, especially for ^{15}N-NO probes, will allow for real-time reaction-based imaging of NO.

1. Introduction

Nitric oxide (NO) is an important gaseous signaling molecule that regulates a wide range of physiological and pathophysiological pathways.[1–3] NO is produced through nitric oxide synthase (NOS)-catalyzed conversion of L-arginine to L-citrulline.[4] Aberrant levels of NO production and NOS expression have been reported in the progression of various cancers, including lung,[5–6] breast,[7–8] and colon cancers.[9–10] Moreover, NO has both pro- and anti-tumorigenic effects that are concentration-dependent, where low concentrations of NO induce cell proliferation and metastasis while high concentrations cause oxidative stress and apoptosis.[11–14] Due to the crucial role of NO and NOS in biological processes, it is of great interest to develop NO sensors to study NO-related physiological pathways and to gain insight into the role of NO in disease progression. An extensive number of NO sensors have been developed, including optical imaging and photoacoustic tomography.[15–25] Although *in vivo* applications have been demonstrated elegantly, these imaging modalities often afford limited capability for noninvasive deep tissue imaging.

Magnetic resonance imaging (MRI) represents a highly attractive combination of unlimited depth penetration and high spatiotemporal resolution. For example, manganese-based paramagnetic complexes have been developed as contrast agents that function as MRI-detectable probes of NO.[26] Different from traditional MRI, Hyperpolarized Nuclear Magnetic Resonance (HP-NMR) offers a powerful approach that addresses the inherently low sensitivity of traditional MRI by artificially inducing large polarizations, thus enabling indirect detection of biological analytes of interest in low concentration through reaction-based detection with a hyperpolarized probe.[27–30] To date, a wide range of molecular probes as useful diagnostic hyperpolarized MRI agents have

* Corresponding authors at: Department of Chemistry, Duke University, Durham, NC 27708, USA (W.S. Warren and Q. Wang).
E-mail addresses: warren.warren@duke.edu (W.S. Warren), qiu.wang@duke.edu (Q. Wang).
[1] These authors contributed equally to this work.

https://doi.org/10.1016/j.bmc.2022.116969
Received 17 May 2022; Received in revised form 9 August 2022; Accepted 16 August 2022
Available online 23 August 2022

been investigated using dissolution Dynamic Nuclear Polarization (dDNP),[31–36] which is known to generate the largest polarization of the solution state hyperpolarization methods so far. Meanwhile, other hyperpolarization techniques have been developed as alternatives that overcome the high-cost expense, long polarization build-up time, and the need for specialized personnel in DNP. For example, Signal Amplification By Reversible Exchange (SABRE) is an inexpensive, fast, and easily implementable alternative to dDNP, and has shown promising development as a clinical hyperpolarization modality.[37–39]

Here we report the design and development of ^{15}N- and ^{13}C-labeled probes as novel HP-MRI NO sensors, and the hyperpolarization study of these isotope-labeled NO-sensing probes using SABRE. This study also allows for direct comparison of the ^{15}N and ^{13}C nuclei performances as hyperpolarized reaction-based probes. The characterizations of the hyperpolarized isotope-labeled probes in this work suggest their potential for sensitive and real-time monitoring of NO, and particularly more favorable properties of ^{15}N-probes in HP-NMR studies.

2. Results and discussion

2.1. Design of ^{15}N- and ^{13}C-labeled 2-aminobiphenyl-5-carbonitrile as HP-NO sensors

The design of hyperpolarizable NO sensing probes is based on the motif of 2-aminobiphenyl-5-carbonitrile (Fig. 1). The 2-aminobiphenyl scaffold is a NO-sensing unit that has been reported for rapid and selective nitric oxide detection through a sensing mechanism that involves nitrosation of aniline in the presence of molecular oxygen, followed by electrophilic aromatic substitution to form the diazo bridge (AZO-products).[22–25] We expect the ^{15}N- and ^{13}C-labeled nitrile group will perform as the signaling unit and the AZO-products generated *in situ* would provide chemical shifts distinguishably different from the ^{15}N- and ^{13}C-labeled 2-aminobiphenyl-5-carbonitriles. Furthermore, the selection of isotopically-labeled nitrile for HP-NMR imaging is founded in the potential for long polarization lifetimes (T_1) in this functional group, which are desirable for a hyperpolarized imaging probe.[38] In this work, we investigate hyperpolarization of both ^{15}N and ^{13}C isotopes as the nitrile functional group allows for direct comparison of the two nuclei that are commonly used for HP-NMR studies.[40–41] Commonly used ^{13}C labeled agents include bioactive metabolites,[42–43] while ^{15}N based agents are more often used in exogenous sensing probes.[44–45] Yet, there has not been a direct comparison of the two isotopes for a hyperpolarized probe that undergo reaction-based sensing of a target analyte. We expect that our reaction-based NO sensors would also make a well-suited comparative study between ^{15}N-labeled and ^{13}C-labeled HP-NMR probes.

2.2. Synthesis and characterization of ^{15}N- and ^{13}C-enriched NO sensing probes

First, we prepared *N, N*-dimethyl probes **^{15}N-I** and **^{13}C-I** to evaluate the chemical shift differences between the two sensors and their resulting AZO-products **^{15}N-I-AZO** and **^{13}C-I-AZO**, respectively (Fig. 2). The ^{15}N-labeled compound **^{15}N-I** had a chemical shift difference of

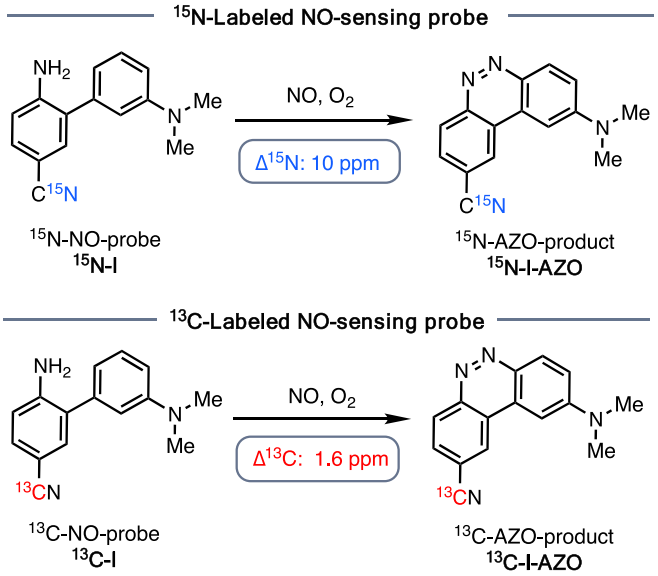

Fig. 2. Dimethyl ^{15}N- and ^{13}C-labeled nitric oxide sensing probes and their respective AZO products.

Δ(^{15}N) = 10 ppm and the ^{13}C-labeled probe **^{13}C-I** had a Δ(^{13}C) = 1.6 ppm. The chemical shift difference for the ^{13}C-labeled probe was smaller than desired, as a large chemical shift change is needed for unambiguous signal detection. However, a large chemical shift for the ^{15}N-probe will facilitate sensitive detection of the NO sensing reaction in clinical MRI (1 T or 3 T).

Based on the encouraging results obtained from **^{15}N/^{13}C-I**, we designed ^{15}N- and ^{13}C-labeled derivatives **^{15}N/^{13}C-II** that bear triethylene glycol (TEG) extensions, which were expected to deliver improved solubility profiles without affecting the core sensing and signaling unit performances (Fig. 3**A**). The TEG-NO probes **^{15}N-II** and **^{13}C-II** were prepared following the synthetic route outlined in Fig. 3**B**. The ^{15}N-4-nitrobenzonitrile **1** was synthesized from condensation of 4-nitrobenzaldehyde with ^{15}NH$_2$OH•HCl, and ^{13}C-4-nitrobenzonitrile **2** was prepared from copper-catalyzed coupling of aryliodide with K^{13}CN in good yields. The isotope-labeled benzonitriles were then subjected to a sequence of nitro reduction, bromination and Suzuki coupling, affording the desired TEG-linked NO probes **^{15}N/^{13}C-II**. This modular synthetic route was expected to not only allow parallel synthesis of both ^{15}N- and ^{13}C-labeled probes, but also to be adaptable for any structural modifications.

To confirm the NO-sensing ability of designed probes, we treated non-isotope-labeled TEG-NO probe **II** with nitric oxide generated *in situ* (via a chemical reaction of $NaNO_2$ with 1 M HCl). The diazotization reaction occurred spontaneously, leading to an instant color change from colorless to a deep red solution. The reaction afforded II-AZO-products in a quantitative yield, as a mixture of *para*- and *ortho*-captured product in a 5:1 ratio (Fig. 3**C**). We also investigated the reaction rate of **II** with NO, which is critical for real-time detection of NO

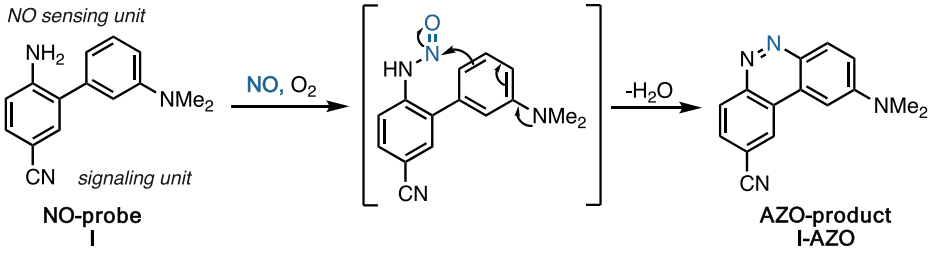

Fig. 1. Design of NO-sensing probes based on the 2-aminobiphenyl-5-carbonitrile motif.

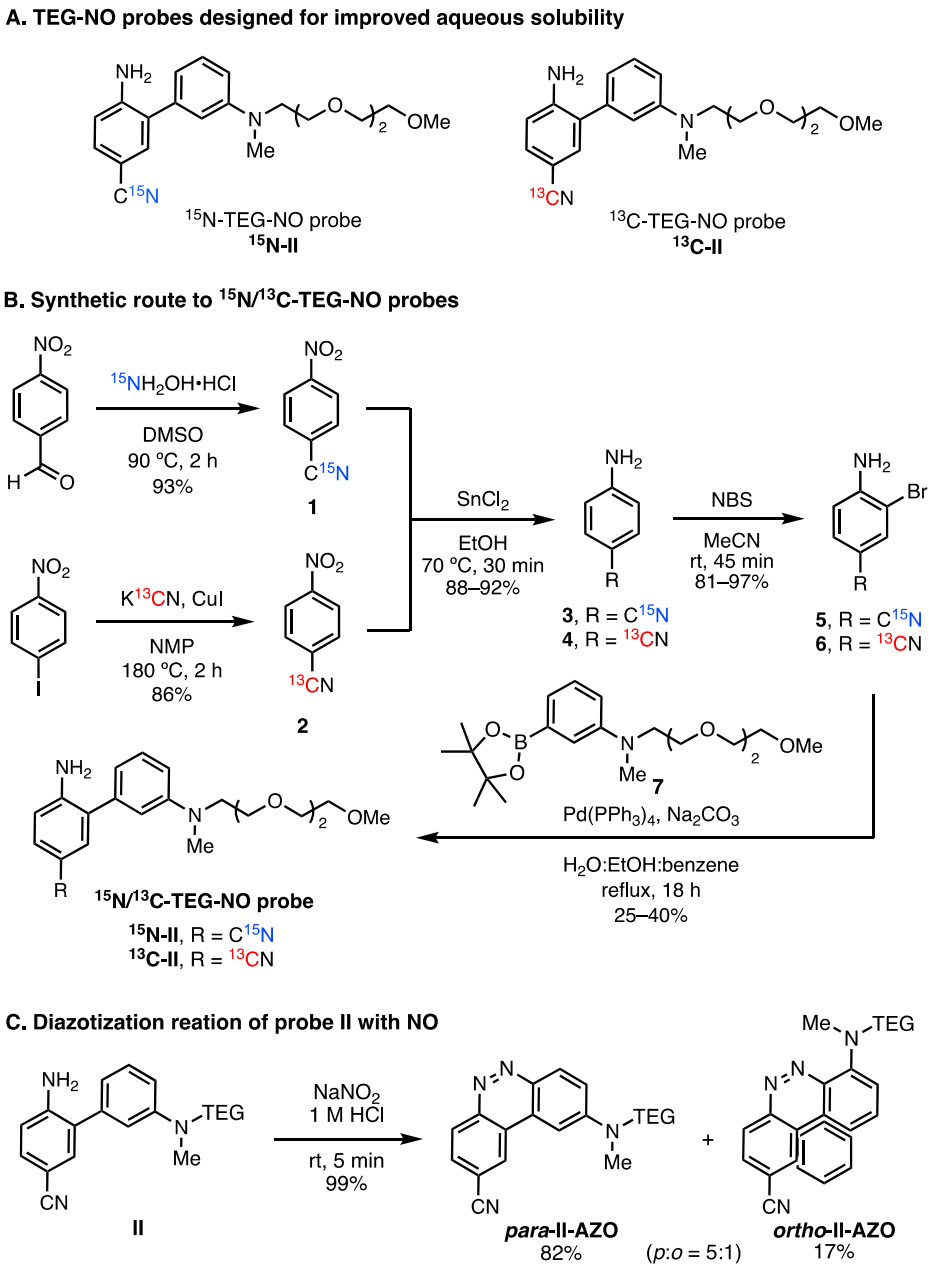

Fig. 3. A) Structures of ^{15}N- and ^{13}C-TEG-NO probes with improved aqueous solubility profiles. B) Synthetic route to ^{15}N-II and ^{13}C-II. C) Reaction of non-labeled TEG-NO probe II with *in situ* generated NO.

that has a short biological lifetime in seconds.[46] Using UV/Vis analysis, we confirmed the completion of diazotization reaction of the TEG-probe **II** with a stock aqueous solution of nitric oxide within 3 mins (Fig. S1).

2.3. SABRE-SHEATH hyperpolarization of NO probes

The potentials of NO-sensing probes for HP-NMR were investigated using the hyperpolarization method, SABRE in SHield Enables Alignment Transfer to Heteronuclei (SABRE-SHEATH), given the simplicity and efficiency of this method. SABRE-SHEATH uses dissolved parahydrogen as a source of spin order to artificially induce large magnetizations on a target nucleus. The parahydrogen and target substrate reversibly interact with an iridium catalytic center to form a polarization transfer complex ($Ir(H)_2(IMes)(pyr)_2$(NO probe)) and a magnetic field in the μT regime is applied to the solution. Under these conditions, the nuclear spin state of the transiently bound system is driven from overpopulation of the singlet state parahydrogen, to overpopulation in the spin up or spin down state on the target nucleus.[47] From the hyperpolarization of the dimethyl probes **^{15}N-I** and **^{13}C-I**, we were delighted to find **^{15}N-I** had spin–lattice relaxation (T_1) value of 7.4 ± 0.6 min with enhancement (ε) of 3300 in d_4-MeOH (1 T) and **^{13}C-I** had T_1 of 59 ± 26 s with a modest ε of 290 (Fig. 4). The short T_1 lifetime of ^{13}C was expected, due to the lower gyromagnetic ratio of ^{13}C compared to that of ^{15}N.[48] Nonetheless, the T_1(^{13}C) is still expected to be long enough for reaction-based imaging.[49]

We next explored hyperpolarization of ^{15}N-TEG-NO probe **^{15}N-II** and ^{13}C-TEG-NO probe **^{13}C-II** in d_6-EtOH, for potentially more biocompatible hyperpolarization conditions (Fig. 5). Although methanol is the common solvent for SABRE experiments, d_6-EtOH has emerged as a more biocompatible SABRE solvent despite a decrease in T_1 value being observed.[50] Hyperpolarization of **^{15}N-II** in d_6-EtOH had T_1 = 2.2 ± 0.2 min and **^{13}C-II** had T_1 = 14.1 ± 5 s. The lower polarization lifetimes observed with **^{15}N/^{13}C-II** compared to the dimethyl analogs are presumably due to the molecular tumbling as well as the solvent effect (d_6-

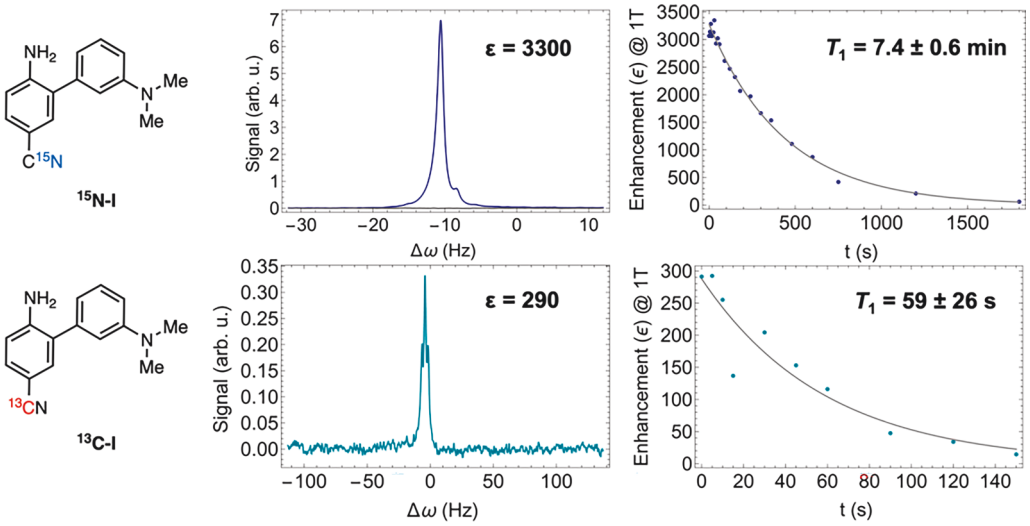

Fig. 4. SABRE-SHEATH hyperpolarization of ^{15}N- and ^{13}C-NO probes **^{15}N-I** and **^{13}C-I** in d_4-MeOH (1 T).

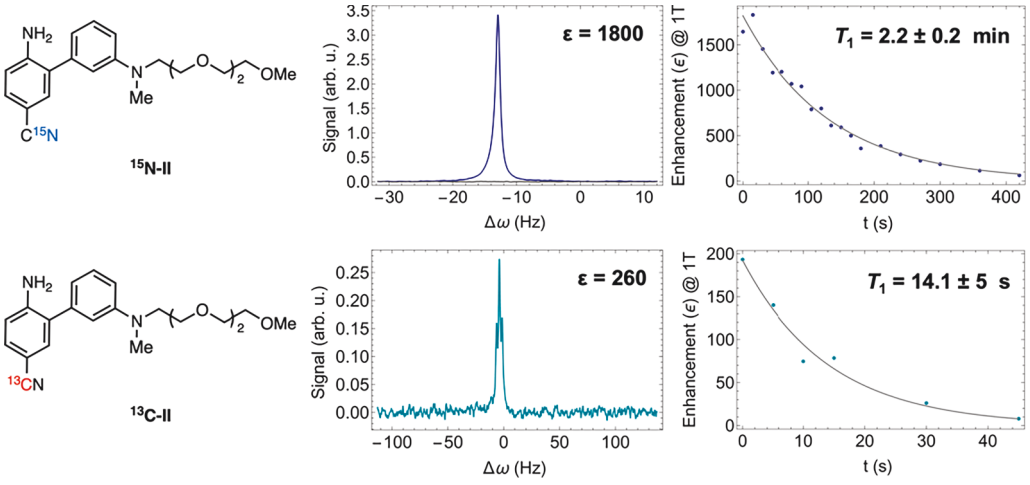

Fig. 5. SABRE-SHEATH hyperpolarization of ^{15}N and ^{13}C-TEG-NO probes **^{15}N-II** and **^{13}C-II** in d_6-EtOH (1 T).

EtOH compared to d_4-MeOH). The addition of the TEG chain increases the size of the probe and potentially reduces the molecular tumbling rate into a more optimal regime for relaxation.

These hyperpolarization studies demonstrate that the lifetimes, chemical shifts, signal enhancement, and nuclear target of hyperpolarized NO-probes are important considerations for reaction-based HP-NMR experiments for direct monitoring of the reaction with NO. Furthermore, monitoring the hyperpolarized signal post-reaction with NO will provide further characterization of the azo products, as direct evaluation of the hyperpolarized azo products is not compatible with SABRE method due to a competing hydrogenation reaction promoted by the SABRE catalyst.

3. Conclusion

In this work, we have designed and synthesized ^{15}N- and ^{13}C-labeled NO sensors that contain 2-aminobiphenyl core as the NO sensing unit and isotope-labeled nitrile as the signal unit for HP-NMR. SABRE-SHEATH hyperpolarization of these NO probes demonstrated long polarization lifetimes that will be critical for efficient NMR imaging studies. While *in vitro/in vivo* imaging has not been demonstrated, this work presents proof of concept of the viability of a reaction-based hyperpolarized ^{15}N- and ^{13}C-labeled NO sensors. The ^{15}N-labeled probes demonstrated larger chemical shift difference (10 ppm versus 1.6 ppm) and longer T_1 lifetimes (in minutes) that are favorable for hyperpolarized imaging studies, compared to those of ^{13}C-labeled probes. These favorable properties make ^{15}N-probes ideal agents for sensitive monitoring of NO using ^{15}N magnetic resonance. Our future work will be focused on hyperpolarized reaction-based imaging of nitric oxide using the ^{15}N-labeled NO probes. We expect that concurrent improvement in the hyperpolarization technique and probe design will lead to future nitric oxide sensing probes that will be applicable to practical *in vivo* studies.

4. Experimental section

4.1. General experimental information

Unless otherwise noted, reactions were performed without exclusion of air or moisture. All commercially available reagents and solvents were used as received unless otherwise stated. Analytical thin-layer chromatography (TLC) was performed using aluminum plates pre-coated with 0.25 mm of 230–400 mesh silica gel impregnated with a fluorescent indicator (254 nm). TLC plates were visualized by exposure to ultraviolet light and/or vanillin and/or $KMNO_4$ stains. Organic solutions were concentrated *in vacuo* using a rotary evaporator. Column

chromatography was performed with silica gel (60 Å, standard grade).

Nuclear magnetic resonance spectra were recorded at ambient temperature on Bruker NEO 500 MHz spectrometer. Proton(^{1}H) chemical shifts are quoted in parts per million (δ) and referenced to the residual internal $CHCl_3$ (δ 7.26). Carbon-13(^{13}C) chemical shifts are referenced to the residual internal $^{13}CHCl_3$ (δ 77.1). The reference point is calculated from the ratios of resonance frequencies following IUPAC recommendations. Resonances are described as s (singlet), d (doublet), t (triplet), q (quartet), quint (quintet), and combinations thereof. Coupling constants (*J*) are given in *Hz* and rounded to the nearest 0.1.

High resolution mass spectra were recorded by the Mass Spectrometry Facility at the Department of Chemistry at Duke University using an Agilent 6224 TOF LC/MS instrument (denoted by LC/ESI). High resolution *m/z* values are reported in Daltons, calculated to 4 decimal points from the molecular formula. All found values are within 5 ppm tolerance. HRMS analyses of compounds containing a bromine atom are based on the isotope of ^{79}Br.

Infrared spectra were recorded on a ThermoScientific Nicolet 6700 FTIR equipped with a diamond ATR. Absorption maxima (ν_{max}) are described as s (strong), m (medium), w (weak), and br (broad) and are quoted in wavenumbers (cm^{-1} Only selected peaks are reported.

4.2. Synthesis of ^{13}C- and ^{15}N-labeled NO probes

4.2.1. 4-nitrobenzonitrile-^{15}N (1)

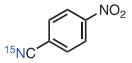

1

To a 25-mL RBF were added 4-nitrobenzaldehyde (300 mg, 2.0 mmol, 1.0 equiv) and $^{15}NH_2OH{\cdot}HCl$ (160 mg, 2.2 mmol, 1.1 equiv). DMSO (1.5 mL) was added and the reaction was heated to 80 °C and stirred for 8 h. The reaction was then cooled to room temp and then poured into H_2O (20 mL), resulting in yellow precipitate. The solid was filtered, washed with H_2O and dried under vacuum to yield the desired product (280 mg, 93%). $\mathbf{R_f}$ = 0.61 (20% EtOAc/hexane); **^{1}H NMR** (500 MHz, $CDCl_3$): δ 8.35 (d, J = 8.8 Hz, 2H), 7.89 (d, J = 8.8 Hz, 2H); **^{13}C NMR** (126 MHz, $CDCl_3$): δ 150.1, 133.6, 124.4, 118.4, 117.0, 116.8; **^{15}N NMR** (51 MHz, $CDCl_3$): δ 263.9; **FTIR** (thin film, DCM): 2207 (w), 1526 (s), 1369 (s) cm^{-1}; **HRMS-ESI**: satisfactory data was unobtainable.

4.2.2. 4-Aminobenzonitrile-^{15}N (3)

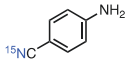

3

To a 4-mL vial was added $SnCl_2$ dihydrate (1.7 g, 7.5 mmol, 5.0 equiv) and EtOH (3.0 mL). To the mixture was added **1** (220 mg, 1.5 mmol, 1.0 equiv) and the resulting dark yellow reaction was heated to 70 °C. After stirring for 40 mins, the reaction was cooled to room temp·H_2O (30 mL) was added and the pH was adjusted to 7–8 with saturated aqueous $NaHCO_3$. The aqueous layer was extracted with EtOAc (10 mL × 3). The combined organic layers were dried over Na_2SO_4, filtered and the filtrate was concentrated *in vacuo* to afford the pure product as yellow solid (160 mg, 92%). **^{1}H NMR** (500 MHz, $CDCl_3$): δ 7.41 (d, J = 8.5 Hz, 2H), 6.54 (d, J = 8.5 Hz, 2H), 4.14 (s, 2H); **^{13}C NMR** (126 MHz, $CDCl_3$): δ 150.5, 134.0, 120.3, 120.1, 114.6, 100.4; **^{15}N NMR** (51 MHz, $CDCl_3$): δ 249.5; **FTIR** (thin film, DCM): 3365 (m), 2163 (m), 1621 (s), 1513 (s), 1320 (s) cm^{-1}; **HRMS-ESI** (*m/z*): Calc'd for $C_7H_7N^{15}N^+$ ($[M + H]^+$): 120.0574; found: 120.0594.

4.2.3. 4-Amino-3-bromobenzonitrile-^{15}N (5)

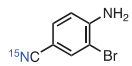

5

To a 25-mL round-bottom flask were added **3** (119 mg, 1.00 mmol, 1.00 equiv) and MeCN (5 mL). *N*-bromosuccinimide (187 mg, 1.05 mmol, 1.05 equiv) and NH_4Cl (5.3 mg, 0.10 mmol, 0.10 equiv) were added and the reaction was stirred at room temperature for 45 min. The reaction was then quenched by the addition of H_2O (10 mL) and extracted with EtOAc (10 mL × 3). The combined organic layers were washed with brine (10 mL), dried over Na_2SO_4, filtered, and the filtrate was concentrated *in vacuo*. The crude was subjected to silica gel chromatography (15% EtOAc/Hexanes) to afford the product as an off-white solid (190 mg, 97%). $\mathbf{R_f}$ = 0.41 (20% EtOAc/hexanes); **^{1}H NMR** (500 MHz, $CDCl_3$): δ 7.70 (d, J = 1.1 Hz, 1H), 7.38 (dd, J = 8.4, 1.1 Hz, 1H), 6.74 (d, J = 8.4 Hz, 1H), 4.61 (s, 2H); **^{13}C NMR** (126 MHz, $CDCl_3$): δ 148.2, 136.6, 132.6, 118.8, 114.9, 108.0, 101.5; **^{15}N NMR** (51 MHz, $CDCl_3$): δ 252.2; **FTIR** (thin film, DCM): 3364 (m), 2190 (m), 1619 (s), 1503 (s) cm^{-1}; **HRMS-ESI** (*m/z*): Calc'd for $C_7H_6BrN^{15}N^+$ ($[M + H]^+$): 197.9679; found: 197.9682.

4.2.4. 4-Nitrobenzonitrile-^{13}C (2)

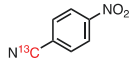

2

To a 50-mL round-bottom flask were added K^{13}CN (177 mg, 2.68 mmol, 1.10 equiv), 1-iodo-4-nitrobenzene (605 mg, 2.43 mmol, 1.00 equiv) and NMP (4 mL). The reaction was heated to 180 °C and stirred for 2 h. The mixture was directly subjected to silica gel chromatography (10% EtOAc/Hexanes) to afford the product (310 mg, 86%). $\mathbf{R_f}$ = 0.61 (20% EtOAc/hexane); **^{1}H NMR** (500 MHz, $CDCl_3$): δ 8.36 (d, J = 8.7 Hz, 2H), 7.89 (dd, J_{C-H} = 8.7, J_{C-C} = 5.2 Hz, 2H); **^{13}C NMR** (126 MHz, $CDCl_3$): δ 149.9, 133.3, 124.2, 117.9, 116.7; **FTIR** (thin film, DCM): 2220 (w), 1532 (s), 1349 (s) cm^{-1}; **HRMS-ESI**: satisfactory data was unobtainable.

4.2.5. 4-Aminobenzonitrile-^{13}C (4)

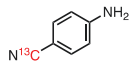

4

To a 4-mL vial was added $SnCl_2$ dihydrate (1.1 g, 4.8 mmol, 4.0 equiv) and EtOH (2.4 mL). To the mixture was added **2** (180 mg, 1.2 mmol, 1.0 equiv) and the resulting yellow reaction was heated to 70 °C. After stirring for 30 mins, the reaction was cooled to room temp·H_2O (25 mL) was added and the pH was adjusted to 7–8 with saturated aqueous $NaHCO_3$. The aqueous layer was extracted with EtOAc (50 mL × 3). The combined organic layers were dried over Na_2SO_4, filtered and the filtrate was concentrated *in vacuo* to afford the pure product as yellow solid (130 mg, 88%). **^{1}H NMR** (500 MHz, $CDCl_3$): δ 7.42 (dd, J = 8.5, 5.1 Hz, 2H), 6.66 (d, J = 8.5 Hz, 2H), 4.20 (s, 2H); **^{13}C NMR** (126 MHz, $CDCl_3$): δ 154.3, 150.3, 133.7, 120.0, 114.3; **FTIR** (thin film, DCM): 3368 (m), 2161 (m), 1604 (s), 1514 (s), 1317 (m) cm^{-1}, **HRMS-ESI** (*m/z*): Calc'd for $C_6^{13}CH_7N_2^+$ ($[M + H]^+$): 120.0637; found: 120.0639.

4.2.6. 4-Amino-3-bromobenzonitrile-^{13}C (6)

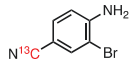

6

To a 15-mL round-bottom flask were added **4** (94 mg, 0.79 mmol, 1.0 equiv) and MeCN (4 mL). *N*-bromosuccinimide (140 mg, 0.79 mmol, 1.0

equiv) and NH_4Cl (4.0 mg, 0.079 mmol, 0.10 equiv) were added and the reaction was stirred at room temperature for 1.5 h. The reaction was then quenched by the addition of H_2O (10 mL) and extracted with EtOAc (15 mL × 3). The combined organic layers were washed with brine (10 mL), dried over Na_2SO_4, filtered, and the filtrate was concentrated *in vacuo*. The crude was subjected to silica gel chromatography (10% EtOAc/Hexanes) to afford the product as an off-white solid (130 mg, 81%). $\mathbf{R_f}$ = 0.41 (20% EtOAc/hexanes); **^{1}H NMR** (500 MHz, $CDCl_3$): δ 7.70 (d, J = 1.1 Hz, 1H), 7.38 (dd, J = 8.4, 1.1 Hz, 1H), 6.74 (d, J = 8.4 Hz, 1H), 4.60 (s, 2H); **^{13}C NMR** (126 MHz, $CDCl_3$): δ 148.3, 136.5, 132.6, 118.7, 114.9 (J_{C-C} = 6.3 Hz), 107.9 (J_{C-C} = 7.4 Hz), 101.2 (J_{C-C} = 85.1 Hz); **FTIR** (thin film, DCM): 3357 (m, br), 2164 (m), 1619 (s), 1502 (s) cm^{-1}; **HRMS-ESI** (*m/z*): Calc'd for $C_6^{13}CH_6BrN_2^+$ ([M + H]$^+$): 197.9742; found: 197.9748.

4.2.7. ^{15}N-dimethyl-NO probe (^{15}N-I)

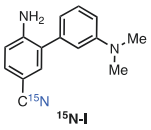

^{15}N-I

To a 50-mL round-bottom flask were added **5** (200 mg, 1.0 mmol, 1.0 equiv), 3-dimethylaminophenyl boronic acid (170 mg, 1.0 mmol, 1.0 equiv), $Pd(PPh_3)_4$ (23 mg, 0.020 mmol, 0.020 equiv) and Na_2CO_3 (850 mg, 8.0 mmol, 8.0 equiv). H_2O (3 mL), EtOH (3 mL) and benzene (10 mL) were added and the resulting milky orange solution was heated to reflux and stirred overnight. The reaction was then cooled to room temperature, diluted with H_2O (20 mL) and extracted with DCM (20 mL × 3). The combined organic layers were dried over Na_2SO_4, filtered, and the filtrate was concentrated *in vacuo*. The crude was subjected to silica gel chromatography (15% EtOAc/Hexanes) to afford the product as a yellow oil (140 mg, 59%). $\mathbf{R_f}$ = 0.34 (20% EtOAc/hexanes); **^{1}H NMR** (500 MHz, $CDCl_3$): δ 7.42 (d, J = 1.7 Hz, 1H), 7.39 (dd, J = 8.3, 1.7 Hz, 1H), 7.33 (t, J = 7.9 Hz, 1H), 6.77–6.71 (m, 4H), 4.32 (s, 2H), 2.99 (s, 6H); **^{13}C NMR** (126 MHz, $CDCl_3$): δ 150.8, 147.8, 137.7, 133.9, 132.1, 129.6, 128.0, 120.1 (J_{C-N} = 18.0 Hz), 116.3, 114.6, 112.3, 111.8, 99.6, 40.2; **^{15}N NMR** (51 MHz, $CDCl_3$): δ 249.6; **FTIR** (thin film, DCM): 3364 (br, w), 2186 (m), 1597 (s), 1492 (s) cm^{-1}; **HRMS-ESI** (*m/z*): Calc'd $C_{15}H_{16}N_2^{15}N$ ([M + H]$^+$): 239.1309; found: 239.1310.

4.2.8. ^{15}N-dimethyl-AZO product (^{15}N-I-AZO)

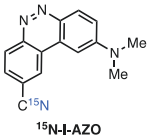

^{15}N-I-AZO

To a 100-mL round bottom flask were added **^{15}N-I** (28 mg, 0.12 mmol, 1.0 equiv) and 1 M HCl (40 mL). The solution was cooled to 0 °C using ice bath and $NaNO_2$ (9.7 mg, 0.14 mmol, 1.2 equiv) dissolved in H_2O (5 mL) was added dropwise, causing the reaction to turn clear yellow to dark red. The resulting mixture was then allowed to warm up to room temperature and stirred for 5 min. The reaction was then neutralized to pH 7 with saturated aqueous $NaHCO_3$ and extracted with DCM (30 mL × 3). The combined organic layers were dried over Na_2SO_4, filtered, and the filtrate was concentrated *in vacuo*. The crude was subjected to silica gel chromatography (100% EtOAc) to afford the product as an orange-red solid (17 mg, 59%). $\mathbf{R_f}$ = 0.34 (20% EtOAc/hexanes); **^{1}H NMR** (500 MHz, $CDCl_3$): δ 8.77 (d, J = 1.5 Hz, 1H), 8.61 (d, J = 8.5 Hz, 1H), 8.50 (d, J = 9.3 Hz, 1H), 7.94 (dd, J = 8.5, 1.5 Hz, 1H), 7.37 (dd, J = 9.3, 2.6 Hz, 1H), 7.26 (d, J = 2.6 Hz, 1H), 3.28 (s, 6H); **^{13}C NMR** (126 MHz, $CDCl_3$): δ 152.5, 145.2, 141.2, 133.3, 131.9, 130.1, 128.1, 122.4, 121.0, 118.7 (d, J_{C-N} = 17.4 Hz), 117.5, 112.8, 97.5, 40.7; **^{15}N NMR** (51 MHz, $CDCl_3$): δ 258.5; **FTIR** (thin film, DCM): 2201 (w), 2143 (w), 1618 (s), 1319 (m) cm^{-1}; **HRMS-ESI** (*m/z*): Calc'd $C_{15}H_{13}N_3^{15}N$ ([M + H]$^+$): 250.1105; found: 250.1107.

4.2.9. ^{13}C-dimethyl-NO probe(^{13}C-I)

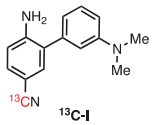

^{13}C-I

Synthesized following the same method as the ^{15}N version using **6** afford the product as an orange-red solid. $\mathbf{R_f}$ = 0.34 (20% EtOAc/hexanes); **^{1}H NMR** (500 MHz, $CDCl_3$): δ 7.40 (d, J = 1.7 Hz, 1H), 7.37 (dd, J = 8.3, 1.7 Hz, 1H), 7.31 (t, J = 7.9 Hz, 1H), 6.75 (dd, J = 8.3, 2.2 Hz, 1H), 6.72–6.68 (m, 3H), 4.38 (s, 2H), 2.99 (s, 6H); **^{13}C NMR** (126 MHz, $CDCl_3$): δ 151.1, 148.0, 138.0, 134.3, 132.4, 129.9, 128.3, 120.3(^{13}CN), 116.5, 114.9, 112.4 (J_{C-C} = 64.3 Hz), 99.9 (J_{C-C} = 84.4 Hz), 40.5. **FTIR** (thin film, DCM): 3366 (br, w), 2161 (m), 1599 (s), 1498 (s) cm^{-1}; **HRMS-ESI** (*m/z*): Calc'd $C_{14}^{13}CH_{16}N_3$ ([M + H]$^+$): 239.1372; found: 239.1372.

4.2.10. ^{13}C-dimethyl-AZO product(^{13}C-I-AZO)

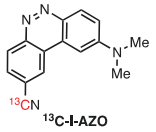

^{13}C-I-AZO

Synthesized following the same method as the ^{15}N version using **^{13}C-I**. **^{1}H NMR** (500 MHz, $CDCl_3$): δ 8.77 (d, J = 1.5 Hz, 1H), 8.61 (d, J = 8.5 Hz, 1H), 8.50 (d, J = 9.3 Hz, 1H), 7.94 (ddd, J = 8.5, 4.5, 1.5 Hz, 1H), 7.37 (dd, J = 9.3, 2.6 Hz, 1H), 7.25 (d, J = 2.6 Hz, 1H), 3.29 (s, 6H); **^{13}C NMR** (126 MHz, $CDCl_3$): δ 152.4, 145.2, 141.2, 133.2, 131. 8, 130.1, 128.1, 122.4, 120.9, 118.7(^{13}CN), 117.5, 113.0, 97.4, 40.6,**FTIR** (thin film, DCM): 2183 (w), 2051 (w), 1612 (s), 1316 (m) cm^{-1}; **HRMS-ESI** (*m/z*): Calc'd $C_{14}^{13}CH_{13}N_4$ ([M + H]$^+$): 250.1168; found: 250.1170.

4.2.11. 3-Bromo-N-(2-(2-(2-methoxyethoxy)ethoxy)ethyl)-N-methylaniline (S1)

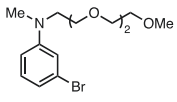

S1

To a 25-mL RBF was added NaH (60% in mineral oil, 96 mg, 2.4 mmol, 1.2 equiv) and DMF (2 mL). 3-bromo-*N*-methylaniline (370 mg, 2.0 mmol, 1.0 equiv) was added at room temperature and the milky grey solution was stirred for 1 h. 1-bromo-2-(2-(2-methoxyethoxy)ethoxy) ethane (500 μL, 2.0 mmol, 1.0 equiv) was added and the resulting mixture was heated to 80 °C and stirred for 18 h. The reaction was then cooled to room temp, EtOAc (20 mL) was added, and the organic layer was washed with 1 M KOH (20 mL × 3). The organic layers were dried over Na_2SO_4, filtered, and the filtrate was concentrated *in vacuo*. The crude was isolated via autocolumn to afford the product (150 mg, 23%). $\mathbf{R_f}$ = 0.31 (40% EtOAc/hexanes); **^{1}H NMR** (500 MHz, $CDCl_3$): δ 7.04 (t, J = 8.2 Hz, 1H), 6.82 (m, 1H), 6.79 (d, J = 7.8, 1H), 6.61 (dd, J = 8.2, 2.2 Hz, 1H), 3.64–3.62 (m, 8H), 3.54–3.50 (m, 4H), 3.38 (s, 3H), 2.96 (s, 3H); **^{13}C NMR** (126 MHz, $CDCl_3$): δ 150.5, 130.4, 123.6, 119.0, 114.9, 110.7, 72.1, 70.9, 70.7, 68.6, 59.2, 52.4, 39.0; **FTIR** (thin film, DCM): 2871 (m, br), 1591 (s), 1493 (s), 1106 (s) cm^{-1}; **HRMS-ESI** (*m/z*): Calc'd for $C_{14}H_{23}BrNO_3^+$ ([M + H]$^+$): 332.0856; found: 332.0862.

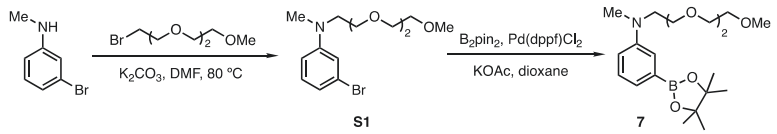

4.2.12. *N-(2-(2-(2-methoxyethoxy)ethoxy)ethyl)-N-methyl-3-(4,4,5,5-tetramethyl-1,3,2-**dioxaborolan**-2-yl)aniline (7)*

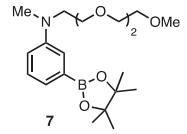

To a 100-mL round bottom flask were added **S1** (1.3 g, 4.0 mmol, 1.0 equiv), bis(pinacolato)diborane (1.1 g, 4.4 mmol, 1.1 equiv), Pd(dppf)Cl_2 (88 mg, 0.12 mmol, 0.030 equiv) and KOAc (1.18 g, 12.0 mmol, 3.00 equiv). 1,4-Dioxane (12 mL) was added and the reaction was heated to 85 °C and stirred overnight. The reaction was then cooled to room temperature, diluted with H_2O (100 mL) and extracted with DCM (70 mL × 3). The combined organic layers were dried over Na_2SO_4, filtered, and the filtrate was concentrated *in vacuo* affording brown oil. The crude was subjected to autocolumn to afford the product as orange oil (840 mg, 56%). $\mathbf{R_f}$ = 0.28 (40% EtOAc/hexanes); **^{1}H NMR** (500 MHz, $CDCl_3$): δ 7.23 (t, J = 8.1 Hz, 1H), 7.15–7.14 (m, 2H), 6.85–6.82 (m, 1H), 3.66–3.62 (m, 8H), 3.57–3.52 (m, 4H), 3.37 (s, 3H), 3.00 (s, 3H), 1.33 (s, 12H); **^{13}C NMR** (126 MHz, $CDCl_3$): δ 148.8, 128.6, 122.9, 118.2, 115.4, 83.7, 72.0, 70.8, 70.7, 70.6, 68.7, 59.1, 52.4, 39.1, 24.9; **FTIR** (thin film, DCM): 2872 (m, br), 1344 (s), 1143 (s), 1104 (s) cm^{-1}; **HRMS-ESI** (*m/z*): Calc'd for $C_{20}H_{35}BNO_5^+$ ([M + H]$^+$): 380.2603; found: 380.2611.

4.2.13. *^{15}N-PEG-NO probe (^{15}N-II)*

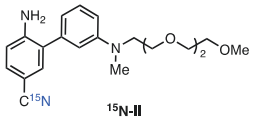

To a microwave tube were added **5** (29 mg, 0.15 mmol, 1.0 equiv), **7** (56 mg, 0.15 mmol, 1.0 equiv), Pd(PPh_3)$_4$ (5.2 mg, 0.0045 mmol, 0.030 equiv) and Na_2CO_3 (130 mg, 1.2 mmol, 8.0 equiv). H_2O (0.5 mL), EtOH (0.5 mL) and benzene (1.6 mL) were added and the resulting solution was heated to reflux and stirred overnight. The reaction was then cooled to room temperature, diluted with H_2O (10 mL) and extracted with EtOAc (10 mL × 3). The combined organic layers were dried over Na_2SO_4, filtered, and the filtrate was concentrated *in vacuo*. The crude was subjected to silica gel chromatography (25–40–80% EtOAc/Hexanes) to afford the product as a yellow oil (22 mg, 40%). $\mathbf{R_f}$ = 0.48 (100% EtOAc); **^{1}H NMR** (500 MHz, $CDCl_3$): δ 7.39–7.37 (m, 2H), 7.29 (t, J = 7.9 Hz, 1H), 6.74–6.66 (m, 4H), 4.40 (br s, 2H), 3.66 (t, J = 5.8 Hz, 2H), 3.61–3.60 (m, 6H), 3.56 (t, J = 5.3 Hz, 2H), 3.52 (dd, J = 5.0, 4.2 Hz, 2H), 3.37 (s, 3H), 3.00 (s, 3H); **^{13}C NMR** (126 MHz, $CDCl_3$): δ 150.0, 148.1, 138.1, 134.3, 132.5, 130.1, 128.3, 120.4, 116.4, 114.9, 112.3, 111.7, 100.1, 72.1, 70.9, 70.8, 70.7, 68.9, 59.1, 52.4, 39.0; **^{15}N NMR** (51 MHz, $CDCl_3$): δ 249.6; **FTIR** (thin film, DCM): 2913 (m, br), 2187 (w), 1599 (s), 1108 (s) cm^{-1}; **HRMS-ESI** (*m/z*): Calc'd for $C_{21}H_{28}N_2^{15}NO_3^+$ ([M + H]$^+$): 371.2096; found: 371.2098.

4.2.14. *^{13}C-PEG-NO probe(^{13}C-II)*

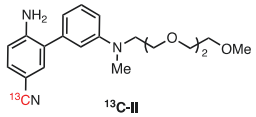

To a microwave tube were added **6** (47 mg, 0.24 mmol, 1.0 equiv), **7** (90 mg, 0.24 mmol, 1.0 equiv), Pd(PPh_3)$_4$ (8.3 mg, 0.0071 mmol, 0.030 equiv) and Na_2CO_3 (200 mg, 1.9 mmol, 8.0 equiv). H_2O (0.9 mL), EtOH (0.9 mL) and benzene (3.0 mL) were added and the resulting solution was heated to reflux and stirred overnight. The reaction was then cooled to room temperature, diluted with H_2O (15 mL) and extracted with EtOAc (15 mL × 3). The combined organic layers were dried over Na_2SO_4, filtered, and the filtrate was concentrated *in vacuo*. The crude was subjected to silica gel chromatography (25–40–80% EtOAc/Hexanes) to afford the product as a yellow oil (28 mg, 25%). $\mathbf{R_f}$ = 0.48 (100% EtOAc); **^{1}H NMR** (500 MHz, $CDCl_3$): δ 7.41–7.36 (m, 2H), 7.29 (t, J = 7.9 Hz, 1H), 6.74–6.66 (m, 4H), 4.40 (br s, 2H), 3.66 (t, J = 5.8 Hz, 2H), 3.62–3.60 (m, 6H), 3.56 (t, J = 5.3 Hz, 2H), 3.52 (dd, J = 5.0, 4.2 Hz, 2H), 3.37 (s, 3H), 3.00 (s, 3H); **^{13}C NMR** (126 MHz, $CDCl_3$): δ 150.0, 148.1, 138.1, 134.4, 132.5, 130.1, 128.3, 120.4, 116.4, 115.0, 112.3, 111.7, 100.5, 72.1, 70.9, 70.8, 70.7, 68.9, 59.1, 52.4, 39.0; **FTIR** (thin film, DCM): 2877 (m, br), 2162 (w), 1599 (s), 1106 (s) cm^{-1}; **HRMS-ESI** (*m/z*): Calc'd for $C_{20}^{13}CH_{28}N_3O_3^+$ ([M + H]$^+$): 371.2159; found: 371.2165.

4.2.15. *II-AZO product*

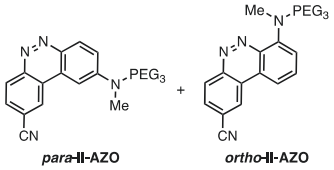

To a 100-mL RBF was added non-labeled **II** (12 mg, 0.032 mmol, 1.0 equiv) and 1 M HCl (10 mL). $NaNO_2$ (3.3 mg, 0.048 mmol, 1.5 equiv) in 0.5 mL H_2O was added dropwise at room temperature, causing the mixture to turn dark red immediately. The starting material was consumed within 1 min based on TLC analysis. After 5 min, the reaction was quenched with $NaHCO_3$ to pH 7–8. The organic layer was extracted with EtOAc (20 mL × 3), and the combined organic layers were dried over Na_2SO_4, filtered, and the filtrate was concentrated *in vacuo*. The crude was purified via autocolumn to afford *ortho*-product (2.1 mg, 17%) and *para*-product (10 mg, 82%).

Ortho-product: $\mathbf{R_f}$ = 0.38 (100% EtOAc); **^{1}H NMR** (500 MHz, $CDCl_3$): δ 8.86 (d, J = 1.6 Hz, 1H), 8.70 (d, J = 8.5 Hz, 1H), 8.00 (dd, J = 8.5, 1.7 Hz, 1H), 7.84–7.77 (m, 2H), 4.10 (t, J = 5.5 Hz, 2H), 4.02 (t, J = 5.5 Hz, 2H), 3.65–3.64 (m, 2H), 3.62–3.60 (m, 4H), 3.53–3.51 (m, 2H), 3.36 (s, 3H), 3.35 (s, 3H); **^{13}C NMR** (126 MHz, $CDCl_3$): δ 151.8, 150.5, 145.2, 133.2, 131.7, 130.1, 128.3, 128.1, 122.6, 121.0, 117.8, 97.8, 72.0, 71.1, 70.8, 70.7, 68.9, 59.1, 52.6, 39.7; **FTIR** (thin film, DCM): 2872 (m, br), 2200 (w), 1609 (s), 1097 (s) cm^{-1}; **HRMS-ESI** (*m/z*): Calc'd for $C_{21}H_{25}N_4O_3^+$ ([M + H]$^+$): 381.1921; found: 381.1910.

Para-product: $\mathbf{R_f}$ = 0.14 (100% EtOAc); **^{1}H NMR** (500 MHz, $CDCl_3$): δ 8.80 (d, J = 1.4 Hz, 1H), 8.62 (d, J = 8.5 Hz, 1H), 8.49 (d, J = 9.3 Hz, 1H), 7.95 (dd, J = 8.5, 1.4 Hz, 1H), 7.45 (dd, J = 9.3, 2.5 Hz, 1H), 7.37 (d, J = 2.5 Hz, 1H), 3.83–3.80 (m, 3H), 3.66–3.62 (m, 4H), 3.60–3.58 (m, 2H), 3.52–3.47 (m, 3H), 3.33 (s, 3H), 3.29 (s, 3H); **^{13}C NMR** (126

MHz, $CDCl_3$): δ 152.0, 145.2, 141.2, 133.2, 131.8, 130.1, 128.1, 122.5, 121.0, 118.8, 117.7, 112.3, 97.7, 72.0, 71.0, 70.7, 68.8, 59.1, 58.3, 52.6, 39.7; **FTIR** (thin film, DCM): 2872 (m, br), 2199 (w), 1607 (s), 1097 (s) cm^{-1}; **HRMS-ESI** (m/z): Calc'd for $C_{21}H_{25}N_4O_3^+$ ($[M + H]^+$): 381.1921; found: 381.1914.

Declaration of Competing Interest

The authors declare that they have no known competing financial interests or personal relationships that could have appeared to influence the work reported in this paper.

Data availability

Data will be made available on request.

Acknowledgements

We acknowledge financial support to this work from NIH (R21 EB024824, P30 CA014236) and NSF (CHE-2003109). We thank Dr. Peter Silinski (Duke University) for the assistance with high-resolution mass spectrometry data.

Appendix A. Supplementary data

Supplementary data to this article can be found online at https://doi.org/10.1016/j.bmc.2022.116969.

References

1 Moncada S. Nitric oxide: discovery and impact on clinical medicine. *J R Soc Med*. 1999;92(4):164–169.
2 Bredt DS, Snyder SH. Nitric oxide: a physiologic messenger molecule. *Annu Rev Biochem*. 1994;63:175–195.
3 Kerwin JF, Lancaster JR, Feldman PL. Nitric Oxide: A New Paradigm for Second Messengers. *J Med Chem*. 1995;38(22):4343–4362.
4 Nathan C, Xie Q-W. Nitric oxide synthases: Roles, tolls, and controls. *Cell*. 1994;78(6):915–918.
5 Ambs S, Bennett WP, Merriam WG, et al. Vascular endothelial growth factor and nitric oxide synthase expression in human lung cancer and the relation to p53. *Br J Cancer*. 1998;78(2):233–239.
6 Okayama H, Saito M, Oue N, et al. NOS2 enhances KRAS-induced lung carcinogenesis, inflammation and microRNA-21 expression. *Int J Cancer*. 2013;132(1):9–18.
7 Thomsen LL, Miles DW, Happerfield L, Bobrow LG, Knowles RG, Moncada S. Nitric oxide synthase activity in human breast cancer. *Br J Cancer*. 1995;72(1):41–44.
8 Glynn SA, Boersma BJ, Dorsey TH, et al. Increased NOS2 predicts poor survival in estrogen receptor–negative breast cancer patients. *J Clin Investig*. 2010;120(11):3843–3854.
9 Ambs S, Merriam WG, Bennett WP, et al. Frequent nitric oxide synthase-2 expression in human colon adenomas: implication for tumor angiogenesis and colon cancer progression. *Cancer Res*. 1998;58(2):334.
10 Ambs S, Bennett WP, Merriam WG, et al. Relationship between p53 mutations and inducible nitric oxide synthase expression in human colorectal cancer. *J Natl Cancer Inst*. 1999;91(1):86–88.
11 Fukumura D, Kashiwagi S, Jain RK. The role of nitric oxide in tumour progression. *Nat Rev Cancer*. 2006;6(7):521–534.
12 Ridnour LA, Thomas DD, Donzelli S, et al. The biphasic nature of nitric oxide responses in tumor biology. *Antioxid Redox Signal*. 2006;8(7–8):1329–1337.
13 Ridnour LA, Thomas DD, Switzer C, et al. Molecular mechanisms for discrete nitric oxide levels in cancer. *Nitric Oxide*. 2008;19(2):73–76.
14 Xu W, Liu LZ, Loizidou M, Ahmed M, Charles IG. The role of nitric oxide in cancer. *Cell Res*. 2002;12(5):311–320.
15 Tsikas D. Analysis of nitrite and nitrate in biological fluids by assays based on the Griess reaction: Appraisal of the Griess reaction in the l-arginine/nitric oxide area of research. *J Chromatogr B*. 2007;851(1):51–70.
16 Wildhirt SM, Dudek RR, Suzuki H, Pinto V, Narayan KS, Bing RJ. Immunohistochemistry in the identification of nitric oxide synthase isoenzymes in myocardial infarction. *Cardiovasc Res*. 1995;29(4):526–531.
17 Matsubara S, Takizawa T, Takayama T, Izumi A, Watanabe T, Sato I. Immuno-electron microscopic localization of endothelial nitric oxide synthase in human placental terminal villous trophoblasts—normal and pre-eclamptic pregnancy. *Placenta*. 2001;22(8):782–786.
18 Kashiwagi S, Izumi Y, Gohongi T, et al. NO mediates mural cell recruitment and vessel morphogenesis in murine melanomas and tissue-engineered blood vessels. *J Clin Investig*. 2005;115(7):1816–1827.
19 Lim MH, Xu D, Lippard SJ. Visualization of nitric oxide in living cells by a copper-based fluorescent probe. *Nat Chem Biol*. 2006;2(7):375–380.
20 Reinhardt CJ, Xu R, Chan J. Nitric oxide imaging in cancer enabled by steric relaxation of a photoacoustic probe platform. *Chem Sci*. 2020;11(6):1587–1592.
21 Reinhardt CJ, Zhou EY, Jorgensen MD, Partipilo G, Chan J. A ratiometric acoustogenic probe for in vivo imaging of endogenous nitric oxide. *J Am Chem Soc*. 2018;140(3):1011–1018.
22 Yang Y, Seidlits SK, Adams MM, et al. A highly selective low-background fluorescent imaging agent for nitric oxide. *J Am Chem Soc*. 2010;132(38):13114–13116.
23 Escamilla PR, Shen Y, Zhang Q, et al. 2-Amino-3′-dialkylaminobiphenyl-based fluorescent intracellular probes for nitric oxide surrogate N2O3. *Chem Sci*. 2020;11:1394–1403.
24 Shen Y, Zhang Q, Qian X, Yang Y. Practical assay for nitrite and nitrosothiol as an alternative to the griess assay or the 2,3-diaminonaphthalene assay. *Anal Chem*. 2015;87(2):1274–1280.
25 Dai C-G, Wang J-L, Fu Y-L, Zhou H-P, Song Q-H. Selective and real-time detection of nitric oxide by a two-photon fluorescent probe in live cells and tissue slices. *Anal Chem*. 2017;89(19):10511–10519.
26 Barandov A, Ghosh S, Li N, et al. Molecular Magnetic resonance imaging of nitric oxide in biological systems. *ACS Sensors*. 2020;5(6):1674–1682.
27 Viale A, Aime S. Current concepts on hyperpolarized molecules in MRI. *Curr Opin Chem Biol*. 2010;14(1):90–96.
28 Ardenkjaer-Larsen JH, Fridlund B, Gram A, et al. Increase in signal-to-noise ratio of > 10,000 times in liquid-state NMR. *Proc Natl Acad Sci*. 2003;100(18):10158–10163.
29 Ardenkjaer-Larsen JH, Boebinger GS, Comment A, et al. Facing and overcoming sensitivity challenges in biomolecular NMR spectroscopy. *Angew Chem Int Ed*. 2015;54(32):9162–9185.
30 Nikolaou P, Goodson BM, Chekmenev EY. NMR Hyperpolarization Techniques for Biomedicine. *Chem Eur J*. 2015;21(8):3156–3166.
31 Comment A. Dissolution DNP for in vivo preclinical studies. *J Magn Reson*. 2016;264:39–48.
32 Gutte H, Hansen AE, Johannesen HH, et al. The use of dynamic nuclear polarization (13)C-pyruvate MRS in cancer. *Am J Nucl Med Mol Imaging*. 2015;5(5):548–560.
33 Hurd RE, Yen Y-F, Chen A, Ardenkjaer-Larsen JH. Hyperpolarized 13C metabolic imaging using dissolution dynamic nuclear polarization. *J Magn Reson*. 2012;36(6):1314–1328.
34 Brindle KM. Imaging metabolism with hyperpolarized 13C-labeled cell substrates. *J Am Chem Soc*. 2015;137(20):6418–6427.
35 Kurhanewicz J, Vigneron DB, Ardenkjaer-Larsen JH, et al. Hyperpolarized (13)C MRI: path to clinical translation in oncology. *Neoplasia*. 2019;21(1):1–16.
36 Wang ZJ, Ohliger MA, Larson PEZ, et al. Hyperpolarized 13C MRI: state of the art and future directions. *Radiology*. 2019;291(2):273–284.
37 Colell JFP, Emondts M, Logan AWJ, et al. Direct hyperpolarization of nitrogen-15 in aqueous media with parahydrogen in reversible exchange. *J Am Chem Soc*. 2017;139(23):7761–7767.
38 Colell JFP, Logan AWJ, Zhou Z, et al. Generalizing, extending, and maximizing nitrogen-15 hyperpolarization induced by parahydrogen in reversible exchange. *J Phys Chem C, Nanomater Interfaces*. 2017;121(12):6626–6634.
39 Rayner PJ, Duckett SB. Signal amplification by reversible exchange (SABRE): From discovery to diagnosis. *Angew Chem Int Ed*. 2018;57(23):6742–6753.
40 Mewis RE, Green RA, Cockett MCR, et al. Strategies for the hyperpolarization of acetonitrile and related ligands by SABRE. *J Phys Chem B*. 2015;119(4):1416–1424.
41 Fekete M, Bayfield O, Duckett SB, et al. Iridium(III) hydrido N-heterocyclic carbene-phosphine complexes as catalysts in magnetization transfer reactions. *Inorg Chem*. 2013;52(23):13453–13461.
42 Keshari KR, Wilson DM. Chemistry and biochemistry of 13C hyperpolarized magnetic resonance using dynamic nuclear polarization. *Chem Soc Rev*. 2014;43(5):1627–1659.
43 Brindle KM, Bohndiek SE, Gallagher FA, Kettunen MI. Tumor imaging using hyperpolarized 13C magnetic resonance spectroscopy. *Magn Reson Med*. 2011;66(2):505–519.
44 Nonaka H, Hata R, Doura T, et al. A platform for designing hyperpolarized magnetic resonance chemical probes. Nat Commun 2013, 4, 2411, Article.
45 Jiang W, Lumata L, Chen W, et al. Hyperpolarized 15N-pyridine Derivatives as pH-Sensitive MRI Agents. *Sci Rep*. 2015;5:9104.
46 Kelm M. Nitric oxide metabolism and breakdown. *Biochim et Biophys Acta (BBA) - Bioenergetics*. 1999;1411(2):273–289.
47 Theis T, Truong ML, Coffey AM, et al. Microtesla SABRE enables 10% nitrogen-15 nuclear spin polarization. *J Am Chem Soc*. 2015;137(4):1404–1407.
48 Harris RK, Becker ED, Cabral de Menezes SM, et al. NMR nomenclature: nuclear spin properties and conventions for chemical shifts: IUPAC recommendations 2001. Solid State Nuclear Magnetic Resonance 2002, 22 (4), 458-483.
49 Note: Attempts to characterize the hyperpolarization of the azo products **^{15}N-I-AZO** and **^{13}C-I-AZO** by SABRE-SHEATH were unfruitful, as the hydrogenation of the azo-bond under SABRE-SHEATH conditions (*para*-H_2 and Ir catalyst) was observed. While this hydrogenation reaction impeded characterization of the hyperpolarized AZO products, it would not impact potential clinical and biological applications of NO probes as the products would not be the target for direct hyperpolarization.
50 Rayner PJ, Burns MJ, Olaru AM, et al. Delivering strong ^{1}H nuclear hyperpolarization levels and long magnetic lifetimes through signal amplification by reversible exchange. *Proc Natl Acad Sci*. 2017;114(16):E3188.